主办 中国科学院遥感与数字地球研究所
中国地理学会环境遥感分会
出版 科学出版社

# JOURNAL OF REMOTE SENSING

# 遥感学报

2013年 Vol.17 第17卷 No.4 第4期 ISSN 1007-4619 CN11-3841 / TP CODEN YXAUAB

## 2010年中国土地覆被遥感监测数据集（ChinaCover2010）

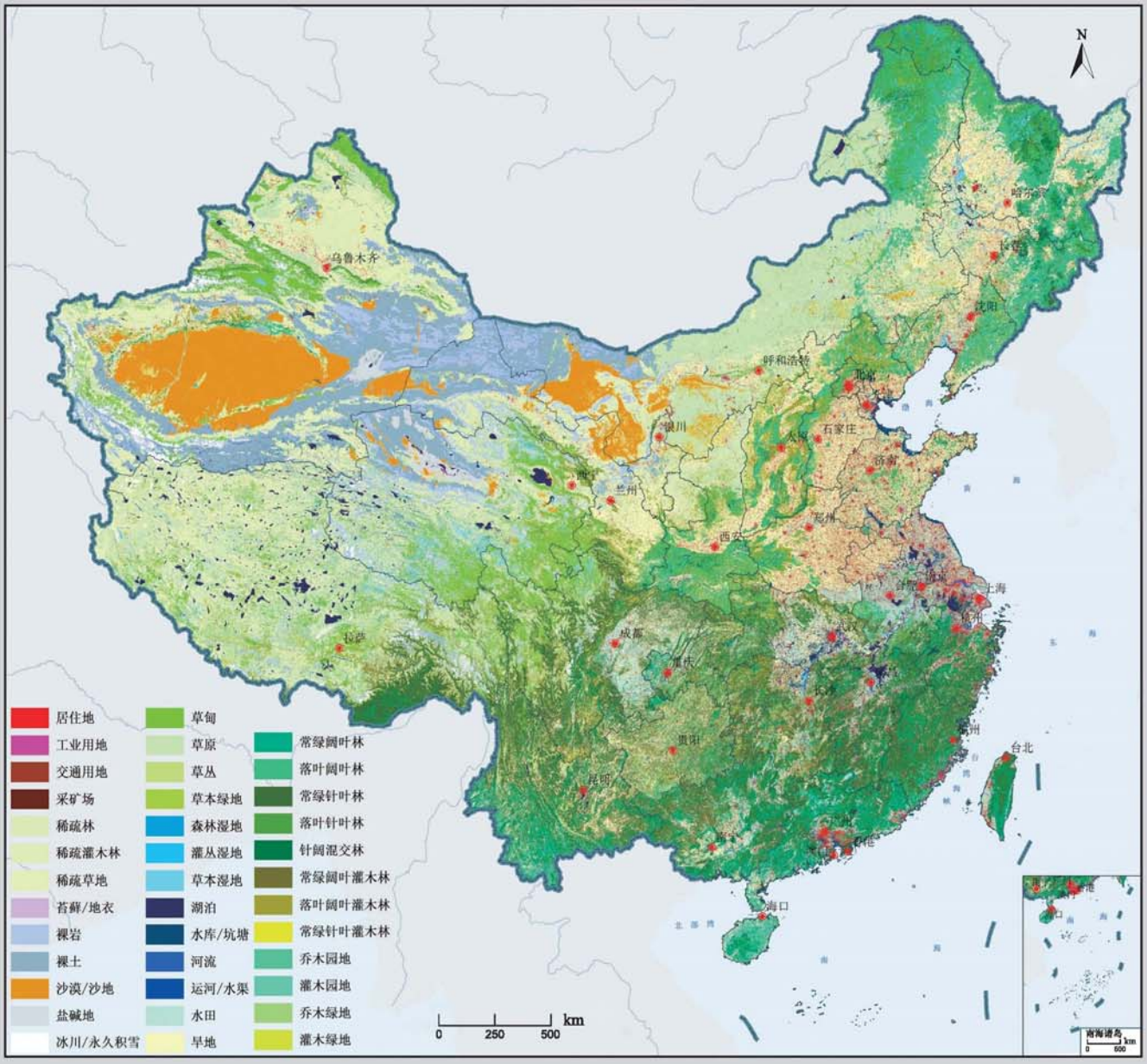

百种中国杰出学术期刊

# 遥感学报

**Yaogan Xuebao**

第 17 卷　　第 4 期　　2013 年 7 月

目　　次

JOURNAL OF REMOTE SENSING

(Vol. 17 No. 4 July, 2013)

## CONTENTS



(to be continued to Inside Back Cover)

(continued from Contents page)

**Haze: Remote Sensing**

# Aerosol optical and microphysical properties in haze days based on ground-based remote sensing measurements

XIE Yisong[1,2], LI Donghui[1,2], LI Kaitao[1,2], ZHANG Long[1,3], CHEN Cheng[1,2], XU Hua[1], LI Zhengqiang[1]

1. *State Environmental Protection Key Laboratory of Satellite Remote Sensing, Institute of Remote Sensing and Digital Earth of Chinese Academy of Sciences, Beijing* 100101, *China*;
2. *University of Chinese Academy of Sciences, Beijing* 100049, *China*;
3. *School of instrument science and optic-electronic engineering, Hefei University of Technology, Hefei* 230009, *China*

**Abstract**: Aerosol optical and microphysical parameters retrieved from ground-based sun-sky photometer (CE318) measurements are used to investigate aerosol properties during heavy haze days. The heavy haze episode in January 2013 is analyzed, and we find that: (1) Aerosol Optical Depth (AOD) in haze days (an average of 0.87 at 440 nm), is much higher than that of clean days, and can reach up to about 3 in some seriously polluted conditions. (2) Aerosol properties are well related to the haze pollution levels. For example, the averaged Ångström exponent, imaginary part of refractive index, single scattering albedo and asymmetry factor under clean condition are 1.3, 0.04, 0.73 and 0.58, respectively, while the corresponding values in polluted days change to 0.95, 0.01, 0.92 and 0.67, respectively. (3) The volume proportion of fine mode aerosol is higher than that of coarse mode during the haze episode. The average volume ratio of fine mode to total aerosol is 73%, with the maximum of 90.5%. The fine mode radius peak increases with the increase of AOD, indicating clearly hygroscopic growth effects, while that of coarse mode aerosol decreases accordingly. Moreover, the peak radius of size distribution is 0.43 μm when the heaviest haze pollution during January 2013 occurs.

**Key words**: sun-sky photometer, Beijing, haze, aerosol, optical and microphysical properties

**CLC number**: TP701 **Document code**: A

**Citation format**: **Xie Y S, Li D H, Li K T, Zhang L, Chen C, Xu H and Li Z Q. 2013. Aerosol optical and microphysical properties in haze days based on ground-based remote sensing measurements. Journal of Remote Sensing, 17(4): 970-980**
[**DOI: 10.11834/jrs.20133060**]

## 1 INTRODUCTION

In recent years, the occurrence of haze polluted weather shows an ascending trend. Both the frequency and pollution level have increased rapidly in industrial regions, especially in urban agglomerations of Beijing-Tianjin-Tangshan, the Yangtze River Delta, and the Pearl River Delta regions (Wang, et al., 2011). Beijing has been suffering serious haze pollution in winters (Li, et al., 2013). Research on aerosol properties in Beijing is useful to understand aerosol impacts on environment, climate and human health.

Previous studies on aerosol optical and microphysical properties from ground-based measurements have shown some aerosol characteristics in haze days. Li, et al. (2013) compared aerosol properties, as well as the remotely sensed component fractions, of two haze events in Beijing during the winters of 2011 and 2012. Yu, et al. (2012) utilized ground-based aerosol observation to analyze the optical properties of haze aerosol. Min, et al. (2009) analyzed the aerosol properties during an obvious haze episode in Xianghe in 2007 based on sunphotometer and lidar observation. Differences of aerosol properties between haze and clean atmosphere were also observed and compared (Yan, et al., 2010; Xu, et al., 2011).

On the basis of above researches, we utilized the sun-sky photometer to acquire aerosol properties in Beijing during the serious haze pollution in January 2013. Aerosol optical parameters like Aerosol Optical Depth (AOD), Ångström exponent ($\alpha$), Single Scattering Albedo (SSA), complex refractive index (real part $m_r$, imaginary part $m_i$), asymmetry factor ($g$), and microphysical parameters (size distribution) are studied. These properties in the haze pollution, as an example, are analyzed in depth to show their variation during the haze process.

**Received**: 2013-03-20; **Accepted**: 2012-05-13; **Version of record first published**: 2013-05-20

**Foundation**: National Major Scientific Research Program (No.2010CB950800, 2010CB950801); National Natural Science Foundation of China (No. 41222007)

**First author biography**: XIE Yisong (1986— ), male, Ph.D. candidate. His research interest is remote sensing of atmospheric aerosol. E-mail: xieys@irsa.ac.cn

**Corresponding author biography**: LI Donghui (1986— ), male, Ph.D. candidate. His research interest is remote sensing of atmospheric aerosol. E-mail: lidh@irsa.ac.cn

## 2 DATA AND METHOD

### 2.1 Instrument and data

The polarized sun-sky photometer (CE-318, manufactured by CIMEL Electronique of Paris, France) is employed to acquire aerosol properties. It has ten channels (0.340 μm, 0.380 μm, 0.441 μm, 0.500 μm, 0.670 μm, 0.870 μm, 0.936 μm, 1.020 μm, 1.020i μm and 1.638 μm) for the aerosol and water vapor observation with the Full Width at Half Maximum (FWHM) of 2 nm (0.34 μm and 0.38 μm) and 10 nm (other channels). The instrument is capable of automatical observation of the direct solar irradiation and sky radiation with ALMucantar (ALM) and Principle Plan (PP) geometries. Large scattering angles are attainable at noon in PP geometry, which measures sky radiation at different solar elevation angles at a fixed solar azimuthal angle. The ALM is superb for providing effective cloud identification for sky radiation which measures symmetrically at different azimuth at a fixed solar zenith. Cloud identification is crucial for data quality control. In this paper we use a limitation of 20% deviation between left ALM (".ALL" files) and right ALM (".ALR" files) measurements (Dubovik, et al., 2000) to identify the cloud. Measurements identified as free of cloud are then averaged and employed in inversion programs (Section 2.2).

The observation site (40°00′N, 116°23′E) is located on the roof of a building (59 m) of Institute of Remote Sensing and Digital Earth (RADI), Chinese Academy of Sciences. We collect effective solar irradiation and sky radiation data from January 1 to 31 in 2013. Some data are excluded due to cloud contamination and precipitation. The meteorological observation data used in this paper are supplied by the Public Meteorological Service of China Meteorological Administration.

The haze pollution in Beijing in January 2013 lasted for about one month, and during this period some extremely polluted days occurred. The entire haze process in January can be further divided into five subprocesses: 6—8, 10—16, 18—19, 21—23, and 25—31, with clear days appearing occasionally. In this paper, the aerosol properties of the entire month are retrieved, and those of the second haze subprocess (10—16) are further analyzed in detail to show the variation during haze process.

### 2.2 Retrieval of aerosol properties

According to Beer-Lambert-Bouguer's law, the relation between photometer measurement and total optical depth can be expressed as

$$V(\lambda) = V_0(\lambda)(d_0/d)^2\exp[-m\tau(\lambda)] \quad (1)$$

where $V(\lambda)$ is the photometer signal at wavelength $\lambda$, $V_0(\lambda)$ is the corresponding calibration coefficient (i.e., the measurement at the top of atmosphere), $\tau(\lambda)$ is the total atmospheric optical depth, $(d_0/d)^2$ is the earth-sun distance correction factor, and $m$ is the aimass that can be calculated from solar zenith. The aerosol optical depth $\tau_a(\lambda)$ can be further calculated by subtracting the Rayleigh optical depth $\tau_R(\lambda)$ and gas absorption optical depth $\tau_g(\lambda)$ from the total optical depth following

$$\tau_a(\lambda) = \tau(\lambda) - \tau_R(\lambda) - \tau_g(\lambda) \quad (2)$$

In Eq.(2), $\tau_R(\lambda)$ can be estimated according to site altitude and $\tau_g(\lambda)$ can be calculated by the 5S model (Tanré, et al., 1990).

Our retrieval approach is an extension of the AErosol RObotic NETwork (AERONET) inversion process (Dubovik, et al., 2000, 2006). AOD calculated from Eq. (2) and sky radiation are used as input parameters in the retrieval. Meanwhile some priori constraints to the parameters are also performed. For example, real part of refractive index is restricted from 1.3 to 1.7, and imaginary part from 0.0005 to 0.5. We retrieved aerosol size distribution and refractive index firstly, and then derived the optical properties such as SSA and asymmetry factor.

## 3 RESULTS AND ANALYSIS

In accordance with AERONET, the standard channels at 440 nm, 675 nm, 870 nm and 1020 nm are selected in the analysis. Fig.1 shows the daily averaged AOD (level 1.5) at Beijing RADI site in January 2013. It is clearly shown that AOD at 440 nm in haze days (0.87) are much larger than that in clear days 0.22. AOD at 440 nm shows extremely rapid increases when haze outbreaks, and the AOD level further reaches up to 2.94 (January 13) and 3.29 (January 27).

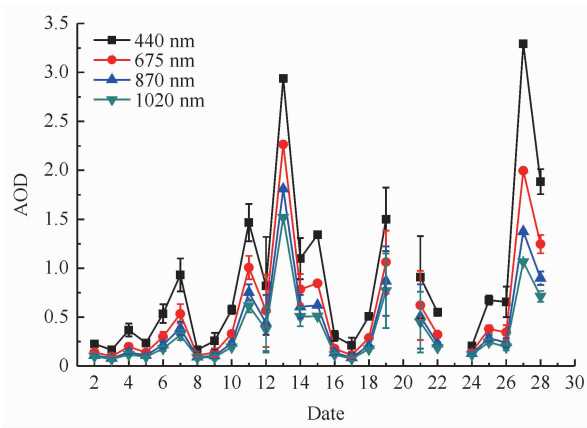


Fig.1 Daily averaged AOD at Beijing RADI site in January 2013 (error bars show the standard deviation)

Daily averaged aerosol parameters are shown in Fig.2(a)—(e), including Ångström exponent (calculated from AOD at 440 nm and 870 nm), SSA (870 nm), refractive index (870 nm), and asymmetry factor (870 nm). The aerosol size distribution is shown in Fig.3.

The Second Haze Subprocess (SHS) is the heaviest and longest one in January 2013. It is thus taken as an example for a detailed quantitative analysis of the variation of the aerosol. We

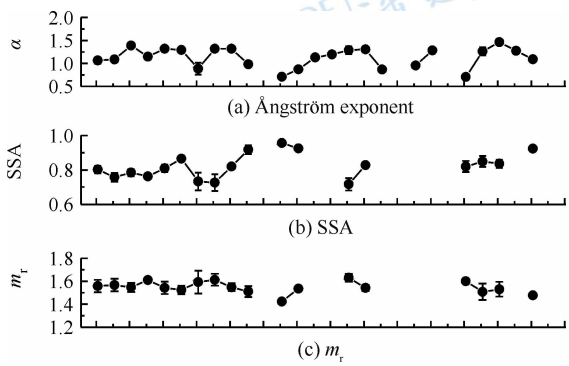

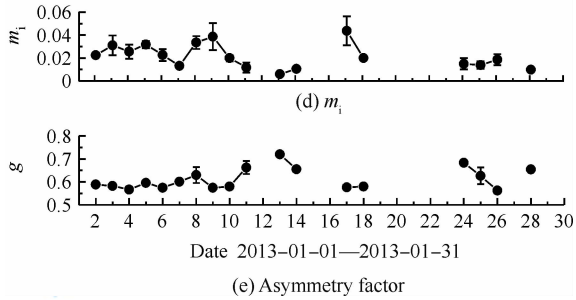


Fig.2 Daily averaged aerosol optical and microphysical properties

add observation of two days under clean condition before (January 9) and after (January 17) the SHS, to show differences between clean and haze conditions.

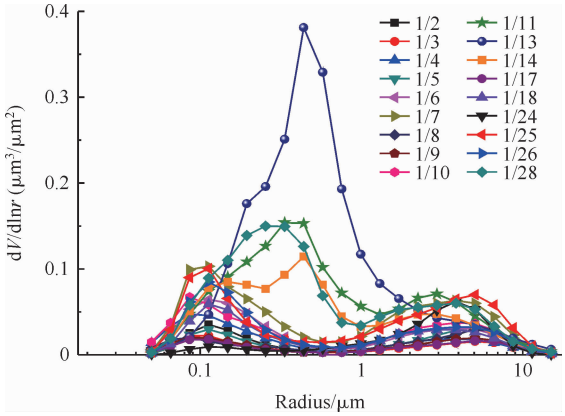


Fig.3 Daily averaged aerosol size distribution in Beijing in January 2013

**Table 1 Aerosol optical and microphysical parameters during the SHS in Beijing in January 2013 (daily averaged)**

| Aerosol parameters | January 9 (clean condition) | January 10—12 (beginning phase) | January 13 (pollution peak) | January 14—16 (cleaning phase) | January 17 (clean condition) |
|---|---|---|---|---|---|
| $\alpha$ | 1.32±0.04 | 1.08±0.03 | 0.70 | 1.07±0.01 | 1.29±0.08 |
| SSA | 0.73±0.05 | 0.89±0.02 | 0.96 | 0.92±0.01 | 0.72±0.04 |
| $m_r$ | 1.61±0.05 | 1.53±0.04 | 1.42 | 1.53±0.02 | 1.63±0.03 |
| $m_i$ | 0.039±0.012 | 0.014±0.003 | 0.006 | 0.011±0.030 | 0.044±0.013 |
| $g$ | 0.57±0.01 | 0.63±0.02 | 0.72 | 0.66±0.01 | 0.58±0.01 |

Table 1 shows the variations of aerosol optical and microphysical properties during the SHS. The retrieval results of January 12, 15, and 16 are not available due to cloud contamination and precipitation. Beyond that, only one retrieval on January 13 is valid.

(1) Ångström exponent

Ångström exponent $\alpha$ is used to describe the spectral dependency of the AOD. It is inversely related to the average size of the aerosol particles in the aerosol, when the number density distribution of aerosol is close to Junge distribution, the larger the particles are the smaller the exponent is (Eck, et al., 1999). In clean atmosphere $\alpha$ is about 1.3, while in the SHS the value decreases to 0.95 (averaged from 10 to 16 in January), indicating the increased average size of particles. This is probably due to aerosol hygroscopic growth (relative humidity of 33%, 69%, 67%, 73%, 75% and 29% for 9—11, 13—14 and 17 in January, respectively). The research of Min, et al. (2009) on Xianghe haze pollution in 2007 showed that Ångström exponent before and during the haze episode were 1.4 and 1 respectively, similar to our results.

(2) Single scattering albedo

Single scattering albedo is the ratio of scattering efficiency to total extinction efficiency. From Table 1 we can see that before the haze pollution SSA is 0.73. SSA increases as the pollution gets heavier, then it reaches up to the peak 0.96, showing the enhanced aerosol scattering in haze atmosphere. SSA decreases to 0.72 when pollution is removed, representing the weakest scattering effect during this period. The average SSA during this haze episode is 0.92, higher than that under clean condition (0.72—0.73), showing similar result with previous work (Min, et al., 2009; Xu, et al., 2011; Yu, et al., 2012). The main reason for the SSA variation might be the transformation of $SO_2$ and $NO_2$ to secondary aerosols such as sulfate and nitrate during haze period. Such transformation greatly enhances the aerosol scattering effect (Yan, et al., 2008) and consequently leads to higher SSA.

(3) Refractive index

Refractive index is the most important optical parameter of aerosol components, the real part $m_r$ indicates the refractivity of aerosol, while the imaginary part $m_i$ indicates the amount of light absorption when the electromagnetic wave propagates through the medium. Before haze pollution, $m_r$ is about 1.61, and decreases to minimum value of 1.42 with the development of pollution. $m_r$ increases again to 1.63 when haze is moved. For the haze days there is an obvious relevance between air humidity and the level of haze pollution. Heavy pollution relates to high water content in aerosol (Wang, et al., 2013), and lower real refractive index as well, considering in aerosol components the refractive index of water (1.33) is the lowest (Dubovik, et al., 2002). The imaginary refractive index $m_i$ shows similar variation trend (decreases in haze developing phase and increases in cleaning phase). The average $m_i$ values are 0.04 and 0.01 under clean condition and haze pollution, respectively, indicating a weak absorption effect of aerosol in haze. This is probably due to increasing secondary aerosols such as sulfate and nitrate (typical value of $m_i$ is 0) during the haze process (Wei, et al., 2013).

(4) Asymmetry factor

Aerosol asymmetry factor $g$ stands for the ratio of forward scattering to the total scattering. The value close to 1 means a large proportion of forward scattering, while the value close to −1 means a large proportion of backward scattering, and the value of 0 means isotropic scattering. The asymmetry factor increases from 0.57 (clean atmosphere, January 9) to 0.72 (pollution peak, January 13) as haze aggravates, and then decreases to 0.58 (clean atmosphere, January 17) in the cleaning phase, showing higher proportion of forward scattering in haze days than that

in clean atmosphere. The average asymmetry factor in haze and clean days are 0.67 and 0.58, respectively. This is probably due to the enlarged size of aerosol particles caused by hygroscopic growth in haze pollution days (Liou, et al., 2002).

(5) Aerosol size distribution

Fig.4 shows the aerosol size distribution of the SHS of haze pollution and Table 2 gives the Volume Concentration (VC) of fine and coarse modes calculated from size distribution.

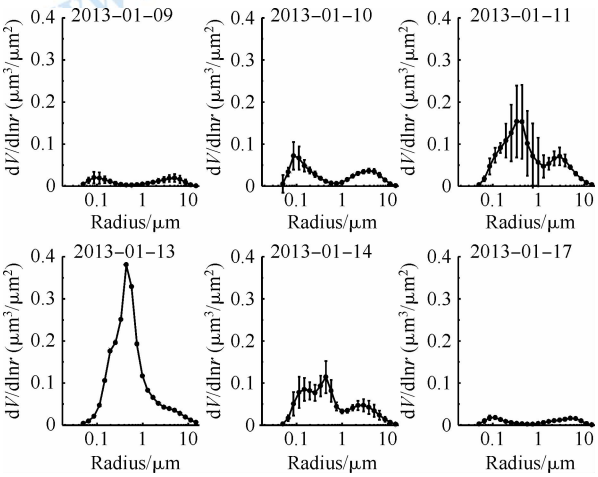


Fig.4 Aerosol size distribution of the SHS (daily averaged)

**Table 2 Volume concentration of fine and coarse mode aerosol ($\mu m^3/\mu m^2$) and AOD (440 nm) of the SHS (daily averaged)**

| Date | VC-fine ($\mu m^3/\mu m^2$) | VC-coarse ($\mu m^3/\mu m^2$) | VC ratio F/C | AOD (440 nm) |
|---|---|---|---|---|
| 01-09 | 0.031±0.014 | 0.038±0.015 | 0.82 | 0.26±0.08 |
| 01-10 | 0.090±0.024 | 0.065±0.009 | 1.38 | 0.58±0.04 |
| 01-11 | 0.279±0.143 | 0.104±0.009 | 2.68 | 1.47±0.19 |
| 01-13 | 0.545 | 0.057 | 9.56 | 2.94 |
| 01-14 | 0.202±0.058 | 0.084±0.024 | 2.39 | 1.10±0.21 |
| 01-17 | 0.025±0.005 | 0.026±0.005 | 0.95 | 0.21±0.08 |

There is an obvious trend in variation of aerosol size distribution with time during the SHS (Fig.4). VC values of fine and coarse modes on 9 January (clean atmosphere) are both very low and show no significant difference, corresponding to relatively small AOD (0.26 at 440 nm). Aerosol shows a bimodal lognormal size distribution, with the peak radii of fine and coarse modes around 0.1 and 3.9 μm respectively. The VC ratio of fine to coarse is about 0.82, illustrating that coarse mode is the dominant mode of aerosol size distribution in Beijing at clean atmosphere, agreeing with previous studies (Yu, et al., 2012). Then VC of both modes increase as haze pollution becomes heavier on 10 and 11 January, along with increasing AOD (0.58 and 1.47 on the two days). This is due to the continuous accumulation of air pollutants in haze days because stable weather system limits the pollutant dispersion. VC of fine mode increases more significantly than the other mode and becomes the dominant mode of the bimodal lognormal size distribution since haze begins. On January 11 the ratio of fine to coarse VC rises to 2.68, and the peak radii of fine and coarse modes change to 0.3 μm and 2.9 μm respectively. The haze pollution reaches its peak on 13 January and VC of total aerosol is 8.7 times of that on January 9. AOD also reaches to the maximum of 2.94 in the SHS, which is about 11 times larger than that in clean atmosphere. The aerosol changes to single mode lognormal distribution with the peak radius at 0.43 μm, and VC ratio of fine to coarse mode is 9.56. VC of fine mode aerosol accounts for 90.5% of the total aerosol. Note that during the haze developing phase, the increasing peak radius of fine mode aerosol is probably caused by the hygroscopic growth effect of soluble aerosols under condition with high humidity (Eck, et al., 2005). After that, VC of the total aerosol begins to decrease from its peak and so does AOD (decreases rapidly to 1.10), due to aerosol particle deposition which might be caused by precipitation on January 14 afternoon. The size distribution reverts to bimodal with peak radii of fine and coarse modes at 0.15 and 2.9 μm respectively. VC of fine mode is still larger than that of coarse mode while VC ratio of fine to coarse mode is 2.39. On January 17, haze pollutants are significantly cleaned up, and VC of both modes and AOD fall to the lowest levels during the SHS, which are comparable with those on January 9. Aerosol shows bimodal lognormal size distribution (with peak radii 0.1 μm and 5.0 μm respectively), similar as that of January 9. The coarse mode dominates the size distribution again, although VC of the two modes are very close and VC ratio of fine to coarse mode is 0.95.

From the variation of the aerosol properties during the haze process (including two clean days), we can see the main pollutants of haze are fine aerosol particles (with radius less than 1.0 μm), while the coarse mode aerosol can also increase a little with aggravation of pollutants. The VC ratio of fine to coarse mode coincides well with AOD at 440 nm in the SHS, indicating significant contribution of fine mode aerosol to the total aerosol optical depth. According to Dubovik, et al. (2002), for urban-industrial aerosol type AOD at 440 nm has higher correlation with fine mode aerosol than coarse mode, in accordance with the results of our work.

## 4 CONCLUSION

We focus on the serious haze pollution in Beijing in January 2013, and use ground-based sun-sky photometer CE-318 measurements to retrieve aerosol optical and microphysical properties, including aerosol optical depth, Ångström exponent, single scattering albedo, refractive index, size distribution and asymmetry factor. The paper analyzes these properties during the second haze subprocess in January 2013 and we conclude that:

(1) AOD at 440 nm reaches to 0.87 during the haze, about four times larger than that of clean days at the same period. The peaks of AOD even reach to 2.94 on January 13 and to 3.29 on January 27.

(2) Aerosol properties are closely related to the haze process. Ångström exponent decreases from 1.3 to 0.95 at pollution period due to hygroscopic growth of soluble aerosol particles. Weakening aerosol absorption effect can lead to decrease of imaginary refractive index (0.04—0.01). Increasing scattering effect of aerosol enlarges single scattering albedo from 0.73 under clean condition to 0.92 during the haze. Asymmetry factor increases by about 15.5% (0.58—0.67), indicating the

enhanced forward scattering in haze days.

(3) In the second haze subprocess, fine mode aerosol is dominant and its VC proportion to the total aerosol is about 90.5% at pollution peak. The aerosol size distribution varies with pollution level during the process, and the VC ratio of fine to coarse mode increases as pollution develops. The average peak radius of fine mode aerosol increases with AOD, indicating the hygroscopic growth effect of aerosol particles, while that of coarse model varies inversely. Aerosol size distribution changes to single mode from bimodal lognormal mode when haze reaches its peak and the peak radius is 0.43 μm.

**Acknowledgements**: The meteorological observation data were kindly offered by Public Meteorological Service of China Meteorological.

## REFERENCES

Dubovik O, Smirnov A, Holben B N, King M D, Kaufman Y J, Eck T F and Slutsker I. 2000. Accuracy assessments of aerosol optical properties retrieved from Aerosol Robotic Network (AERONET) Sun and sky radiance measurements. Journal of Geophysical Research, 105(D8): 9791-9806 [DOI: 10.1029/2000JD900040]

Dubovik O, Holben B N, Eck T F, Smirnov A, Kaufman Y J, King M D, Tanré D and Slutsker I. 2002. Variability of absorption and optical properties of key aerosol types observed in worldwide locations. Journal of the Atmospheric Sciences, 59(3): 590-608 [DOI: 10.1175/1520-0469(2002)059<0590:VOAAOP>2.0.CO;2]

Dubovik O, Sinyuk A, Lapyonok T, Holben B N, Mishchenko M, Yang P, Eck T F, Volten H, Muñoz O, Veihelmann B, van der Zande W J, Leon J F, Sorokin M and Slutsker I. 2006. Application of spheroid models to account for aerosol particle nonsphericity in remote sensing of desert dust. Journal of Geophysical Research, 111(D11) [DOI: 10.1029/2005JD00661 9]

Eck T F, Holben B N, Reid J S, Dubovik O, Smirnov A, O'Neill N T, Slutsker I and Kinne S S. 1999. Wavelength dependence of the optical depth of biomass burning, urban, and desert dust aerosols. Journal of Geophysical Research, 104(D24): 31333-31349 [DOI: 10.1029/1999JD900923]

Eck T F, Holben B N, Dubovik O, Smirnov A, Goloub P, Chen H B, Chatenet B, Gomes L, Zhang X Y, Tsay S C, Ji Q, Giles D and Slutsker I. 2005. Columnar aerosol optical properties at AERONET sites in central eastern Asia and aerosol transport to the tropical mid-Pacific. Journal of Geophysical Research, 110(D6) [DOI: 10.1029/2004jd005274]

Li Z, Gu X, Wang L, Li D, Li K, Dubovik O, Schuster G, Goloub P, Zhang Y, Li L, Xie Y, Ma Y and Xu H. 2013. Aerosol physical and chemical properties retrieved from ground-based remote sensing measurements during heavy haze days in Beijing Winter. Atmospheric Chemistry and Physics Discussion, 13(2): 5091-5122 [DOI: 10.5194/acpd-13-5091-2013]

Li Z Q, Xu H, Zhang Y, Zhang Y H, Chen C, Li D H, Li L, Hou W Z, Lü Y and Gu X F. 2013. Joint use of active and passive remote sensing for monitoring of severe haze pollution in Beijing 2013. Journal of Remote Sensing, 17(4): 919-928 [DOI:10.11834/jrs.20133066]

Liao K N. 2002. An Introduction to Atmospheric Radiation 2nd edn. Beijing: China Meteorological Press: 6-8

Min M, Wang P C, Zong X M, Xia J R and Meng X Y. 2009. Observation and study on aerosol properties in hazy days. Climatic and Environmental Research, 14(2): 153-160

Tanré D, Deroo C, Duhaut P, Herman M, Morcrette J J, Perbos J and Deschamps P Y. 1990. Technical note Description of a computer code to simulate the satellite signal in the solar spectrum: the 5S code. International Journal of Remote Sensing, 11(4): 659-668 [DOI: 10.1080/01431169008955048]

Wang L, Li Z Q, Ma Y, Li L and Wei P. 2013. Retrieval of aerosol chemical composition from ground-based remote sensing data of sun-sky radiometers during haze days in Beijing Winter. Journal of Remote Sensing, 17(4): 944-958 [DOI:10.11834/jrs.20133059]

Wang X Q, Yang T and Wang Z F. 2011. Impact of dust-haze episode from one air pollution control region to the other-one case study. Climatic and Environmental Research, 16(6): 690-696

Wei P, Wang Y, Xie Y S, Li Z Q, Zhang Y and Xu H. 2013. Remote sensing estimation of aerosol chemical composition and radiative effects in haze days. Journal of Remote Sensing, 17(4): 1021-1031 [DOI:10.11834/jrs.20133080]

Xu Z, Li W J, Yu Y C, Wang X F, Zhou S Z and Wang W X. 2011. Characteristics of aerosol optical properties at haze and non-haze weather during autumn at Jinan city. China Environmental Science, 31(4): 546-552

Yan P, Tang J, Huang J, Mao J, Zhou X, Liu Q, Wang Z and Zhou H. 2008. The measurement of aerosol optical properties at a rural site in Northern China. Atmospheric Chemistry and Physics, 8(8): 2229-2242

Yu X N, Li X M, Deng Z R D, De Q Y Z and Yuan S. 2012. Optical properties of aerosol during haze-fog episodes in Beijing. Environmental Science, 33(4): 1057-1062

# 基于地基遥感的灰霾气溶胶光学及微物理特性观测

谢一凇[1,2]，李东辉[1,2]，李凯涛[1,2]，张龙[1,3]，陈澄[1,2]，许华[1]，李正强[1]

1.中国科学院遥感与数字地球研究所 国家环境保护卫星遥感重点实验室，北京 100101；

2.中国科学院大学，北京 100049；

3.合肥工业大学 仪器科学与光电工程学院，安徽 合肥 230009

**摘　要**：为了解北京地区2013年1月严重灰霾污染过程中大气气溶胶特性，基于地基太阳-天空辐射计CE318观测数据，反演了气溶胶光学和微物理参数，并据此对1月份第2次严重污染过程进行了详细分析。研究表明：(1)2013年1月北京地区灰霾污染天气下，气溶胶光学厚度比同时期清洁天气有所增大，在440 nm处均值达到0.87，在个别严重污染天气下高达3左右；(2)气溶胶光学参数与灰霾过程密切相关，Ångström指数由清洁大气时的1.3降到灰霾污染时的0.95，复折射指数虚部均值由污染前的0.04下降为污染过程中的0.01，单次散射反照率均值则由0.73增大到0.92，同时不对称因子均值从0.58增大到0.67；(3)灰霾污染过程中细模态气溶胶比例较高，占总体积比例平均达到73.0%，最高达90.5%，在灰霾污染中气溶胶细模态平均峰值半径随光学厚度增大而增大，清楚表明了灰霾过程中颗粒物的吸湿增长效应，粗模态平均峰值半径随光学厚度的增加而减小，在污染最严重时，粒子谱分布峰值半径约为0.43 μm。

**关键词**：地基太阳-天空辐射计，北京，灰霾，气溶胶光学与微物理特征

**中图分类号**：TP701　　**文献标志码**：A

**引用格式**：谢一凇，李东辉，李凯涛，张龙，陈澄，许华，李正强. 2013. 基于地基遥感的灰霾气溶胶光学及微物理特性观测. 遥感学报，17(4)：970-980

Xie Y S, Li D H, Li K T, Zhang L, Chen C, Xu H and Li Z Q. 2013. Aerosol optical and microphysical properties in haze days based on ground-based remote sensing measurements. Journal of Remote Sensing, 17(4): 970-980

[DOI: 10.11834/jrs.20133060]

## 1　引　言

近年来，中国许多大城市的灰霾污染天气，无论是天数还是严重程度都呈现出加剧趋势，特别是在工业集中、经济发达的京津唐、长三角、珠三角等地区，都出现了严重的区域性大气污染(王喜全等，2011)。北京市自2008年奥运会之后，已多次出现严重的灰霾污染事件(Li等，2013)。北京是中国华北地区灰霾污染天气出现频率较高的城市，因此研究北京地区灰霾天气中气溶胶特性的变化，对进一步了解该区域气溶胶特性及其对环境、气候变化的影响，有重要的意义。

针对中国北方城市灰霾天气，已有学者利用地基观测资料对气溶胶光学及微物理特性做了一些研究。Li等人(2013)对比分析了北京地区2011年和2012年冬季两次灰霾过程中的气溶胶特性，并据此反演分析了灰霾中气溶胶组成成分；于兴娜等人(2012)利用气溶胶地基观测数据分析了北京地区雾霾期间气溶胶光学特性；闵敏等人(2009)基于太阳光度计和激光雷达观测资料，对香河县一次灰霾过程中气溶胶特性进行了分析；Yan等人(2010)对比分析了上甸子观测站雾霾期间和清洁时段气溶胶光学特性；徐政等人(2011)根据黑碳仪和积分浊度计观测数据对比了济南秋季霾与非霾天气下气溶胶光学特性。

本文在上述研究工作的基础上，针对2013年1月份北京地区出现的重度灰霾污染天气(李正强等，2013)，利用太阳-天空辐射计CE318观测数据进

**收稿日期**：2013-03-20；**修订日期**：2013-05-13；**优先数字出版日期**：2013-05-20

**基金项目**：国家重大科学研究计划(编号：2010CB950800，2010CB950801)；国家自然科学基金(编号：41222007)

**第一作者简介**：谢一凇(1986— )，男，博士研究生，专业为地图学与地理信息系统，现从事大气气溶胶观测与反演研究。E-mail: xieys@irsa.ac.cn

**通信作者简介**：李东辉(1986— )，男，博士研究生，主要从事大气气溶胶观测与反演研究。E-mail: lidh@irsa.ac.cn

行了气溶胶参数的计算和反演,包括光学参数如气溶胶光学厚度 AOD(Aerosol Optical Depth)、Ångström 指数 $\alpha$、单次散射反照率 SSA(Single Scattering Albedo)、复折射指数(实部 $m_r$,虚部 $m_i$)、不对称因子 $g$,与微物理参数粒子体积谱分布,并针对 2013 年 1 月第 2 次严重灰霾过程中气溶胶光学和微物理特性进行了详细分析。

## 2 数据与方法

### 2.1 观测仪器与数据

本研究所采用的观测仪器是偏振类型的太阳-天空辐射计 CE318(法国 CIMEL 公司制造)。该仪器共有 10 个通道(0.340 μm、0.380 μm、0.441 μm、0.500 μm、0.674 μm、0.870 μm、0.936 μm、1.020 μm、1.020i μm 和 1.638 μm),各通道 FWHM(Full Width at Half Maximum)为 2—10 nm(紫外通道 0.340 μm 与 0.380 μm 是 2 nm,其他通道是 10 nm),能实现无人值守自动化运行。仪器观测方式包括太阳直射光和天空光观测。在天空光的观测方式上,该仪器采用太阳主平面扫描 PP(Principle Plan)和平纬圈扫描 ALM(ALMucantar)两种方式。PP 是对同一太阳方位角做不同天顶角的天空光观测,这种观测方式容易在正午获得较大散射角。ALM 则是观测同一太阳天顶角不同方位角的天空光,其主要优势是能利用观测对称性进行云污染的判断。云污染检测技术是确保研究数据质量的关键,本文采用的标准是以太阳为中心的左平纬圈(原始数据中的".ALL"类型数据)和右平纬圈(原始数据中的".ALR"类型数据)观测数值相差小于 20%(Dubovik 等,2000)。通过云检测的观测点数据,将数值平均后加入到反演程序中。

本研究用到的太阳-天空辐射计架设在中科院遥感与数字地球所楼顶(40.0048°N,116.3786°E,海拔为 59 m)。观测时间为 2013-01-01 至 2013-01-31。其中,由于云和降水等天气原因,仪器无有效记录数据或自动停止观测,因此有部分时间段数据缺失。本文用到的气象观测数据,来自于中国气象局公共气象服务中心。

2013 年 1 月北京地区灰霾污染呈现持续时间长,污染程度严重的特点,并且在污染过程中间歇出现清洁天气。整个灰霾污染过程主要可分为 5 个子过程:1 月 6 日—8 日、10 日—16 日、18 日—19 日、21 日—23 日和 25 日—31 日。本文对整个 1 月份观测数据进行了气溶胶特性参数反演,并以第 2 次灰霾污染过程为例进行详细分析。

### 2.2 气溶胶光学及微物理参数反演

根据 Lambert-Beer 定律,太阳辐射计在窄波段 $\lambda$ 处地表的观测值 $V(\lambda)$,可以表示为:

$$V(\lambda) = V_0(\lambda)(d_0/d)^2 \exp[-m\tau(\lambda)] \quad (1)$$

式中,$V_0(\lambda)$ 为大气层顶的观测值,即仪器定标常数,$\tau(\lambda)$ 是总的大气光学厚度,$(d_0/d)^2$ 为日地距离修正因子,$m$ 为大气质量数,可通过太阳天顶角来计算。根据式(1)可以计算出总的光学厚度 $\tau(\lambda)$,并根据式(2)计算出气溶胶光学厚度:

$$\tau_a(\lambda) = \tau(\lambda) - \tau_R(\lambda) - \tau_g(\lambda) \quad (2)$$

式中,$\tau_a(\lambda)$ 为所求的气溶胶光学厚度,等号右边后两项分别为瑞利分子光学厚度 $\tau_R(\lambda)$ 和吸收气体光学厚度 $\tau_g(\lambda)$。瑞利分子光学厚度可通过海拔高度来计算求出,吸收气体光学厚度可通过 5S 模型(Tanré 等,1990)计算得到。

本文采用的气溶胶光学和微物理特性反演算法是在地基气溶胶观测网 AERONET(AErosol RObotic NETwork)算法(Dubovik 等,2000,2006)基础上扩展而成。该反演算法利用光学厚度和经过定标的天空辐亮度作为输入参数,同时对要反演的气溶胶参数进行边界先验约束。例如,复折射指数实部和虚部反演范围分别为 1.3—1.7 和 0.0005—0.5。利用该方法首先得到微物理参数粒子体积谱分布和光学参数复折射指数,然后计算得到其他的光学参数,如单次散射反照率和不对称因子等。

## 3 结果与分析

为了与 AERONET 保持一致,本文挑选 440 nm、675 nm、870 nm 和 1020 nm 4 个波段进行分析。图 1 显示了 2013 年 1 月份北京 RADI 站点的 AOD 日均值(level 1.5)观测结果,可以看出,2013 年 1 月北京地区气溶胶光学厚度较大,440 nm 处的 AOD 均值达到 0.87,而在本月清洁天气下 AOD 均值只有 0.22。另外伴随着灰霾污染的爆发,AOD 多次出现急剧增大,在个别严重污染天气下达 2.94(1 月 13 日)和 3.29(1 月 27 日)。

图 2(a)—(e)分别显示了 2013 年 1 月份经过云剔除的各参数日均值反演结果,包括:Ångström 指数(采用 440/870 nm 计算)、单次散射反照率(870 nm)、复折射指数(870 nm)和不对称因子(870 nm)。图 3 显示了相应的气溶胶粒子体积谱分布的反演结果。第 2 次灰霾污染(1 月 10 日—16 日)是 5 次子过

程中程度最严重的，并且持续时间长，具有较好的典型性。本节以该次污染为例，说明北京地区灰霾污染过程中大气气溶胶的光学特性，并加入本次污染过程前后的清洁天气观测(1 月 9 日和 1 月 17 日)作为对比。

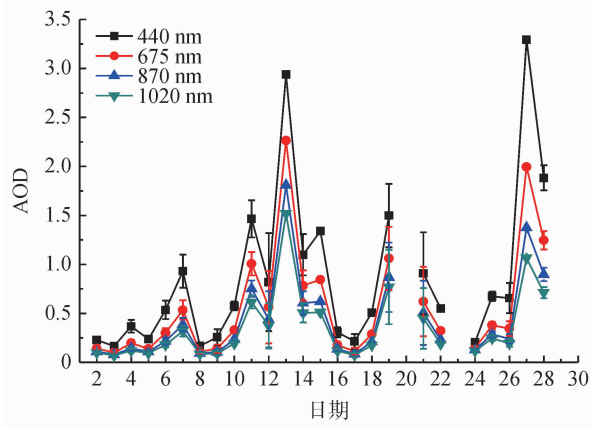


图 1　北京 RADI 站点 2013 年 1 月气溶胶光学厚度观测结果
(误差线显示计算日平均值时的标准偏差)

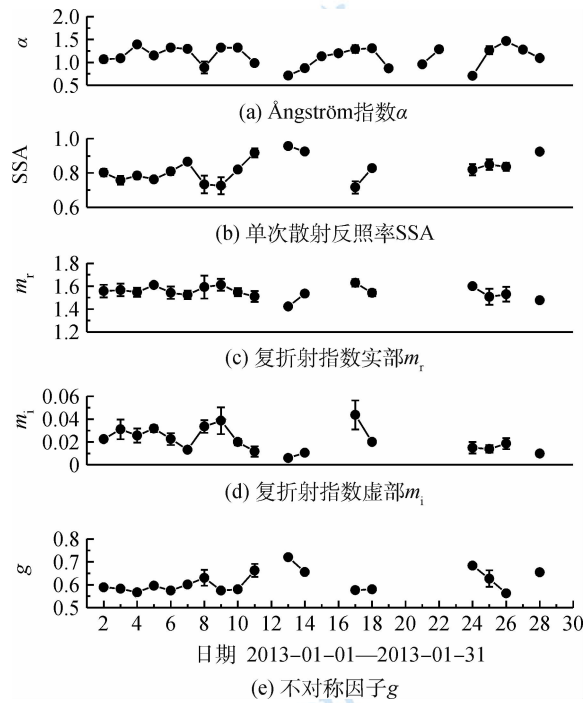


图 2　气溶胶光学与微物理参数反演结果(日均值)

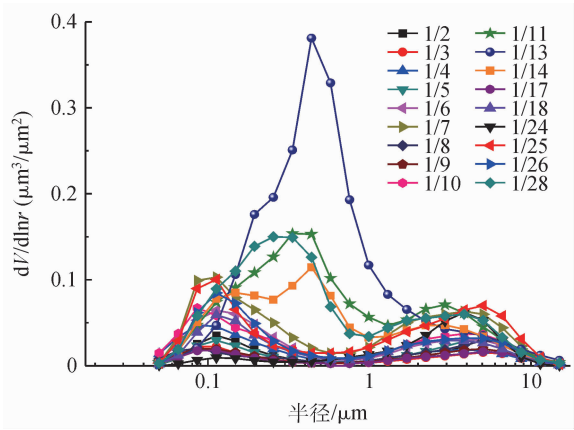


图 3　气溶胶粒子体积谱分布反演结果(日均值)

表 1 显示了上述几种气溶胶光学和微物理参数在第 2 次灰霾严重污染过程中的变化情况，其中“±”后数字表示标准差。1 月 12 日、15 日、16 日由于天气原因没有反演结果，1 月 13 日只有一组反演结果。

(1)Ångström 指数

Ångström 指数 α 是用来描述气溶胶光学厚度随波长变化关系的物理量。当气溶胶粒子数谱分布接近容格谱时，α 可以反映气溶胶粒子大小，粒子尺度越大，α 值越小(Eck 等，1999)。从本次灰霾发展过程来看，α 在清洁天气的值约为 1.3，而在整个灰霾污染期间均值(1 月 10 日—16 日平均值)约为 0.95。α 值的减小表明粒子平均尺度有所增大，从图 3 中也可明显看出。这可能是由于本次灰霾过程中相对湿度较大(1 月 9 日—11 日，13 日—14 日，17 日的相对湿度依次为 33%、69%、67%、73%、75% 和 39%)，气溶胶粒子发生吸湿增长，体积增大。闵敏等人(2009)研究 2007 年 4 月香河地区灰霾过程时发现 Ångström 指数在灰霾前和灰霾爆发时分别为 1.4 和 1 左右，与本文研究结果相近。

(2)单次散射反照率

单次散射反照率 SSA 反映了气溶胶粒子总体消光中散射所占的比例。可以看出，SSA 在灰霾爆发之前为 0.73，随着灰霾污染的发展逐渐变大，峰值

**表 1　北京地区 2013 年 1 月第 2 次严重灰霾污染过程中气溶胶光学及微物理参数(日均值)**

| 气溶胶参数 | 1 月 9 日<br>(清洁天气) | 1 月 10 日至 12 日<br>(开始与发展) | 1 月 13 日<br>(污染峰值) | 1 月 14 日至 16 日<br>(减少与清除) | 1 月 17 日<br>(清洁天气) |
|---|---|---|---|---|---|
| α | 1.32±0.04 | 1.08±0.03 | 0.70 | 1.07±0.01 | 1.29±0.08 |
| SSA | 0.73±0.05 | 0.89±0.02 | 0.96 | 0.92±0.01 | 0.72±0.04 |
| $m_r$ | 1.61±0.05 | 1.53±0.04 | 1.42 | 1.53±0.02 | 1.63±0.03 |
| $m_i$ | 0.039±0.012 | 0.014±0.003 | 0.006 | 0.011±0.030 | 0.044±0.013 |
| g | 0.57±0.01 | 0.63±0.02 | 0.72 | 0.66±0.01 | 0.58±0.01 |

为0.96,增大约31.5%,说明气溶胶散射作用伴随着污染过程增强,之后SSA逐渐减小至污染结束时的0.72,相应的散射作用也降到最低。整个灰霾污染过程中SSA均值约为0.92,明显高于清洁大气的数值0.72—0.73,这与前人关于灰霾污染中SSA变化的研究结果相近(闵敏 等,2009;徐政 等,2011;于兴娜 等,2012)。导致灰霾污染期间SSA出现这种变化的原因主要是在灰霾影响下,$SO_2$、$NO_2$等气体转化为对应的二次气溶胶硫酸盐、硝酸盐,使气溶胶散射能力有所提高(Yan 等,2008)。

(3)复折射指数

气溶胶复折射指数是反映气溶胶成分特征最主要的光学常数,其实部$m_r$是气溶胶的折射率,表征气溶胶散射特征;其虚部$m_i$表征气溶胶的吸收特征。$m_r$从清洁大气的1.61,随灰霾的发展逐渐减小至谷值1.42,之后随着污染清除逐渐增大至1.63。通常,在灰霾过程中,空气相对湿度与灰霾污染程度有较好的相关性,灰霾污染中气溶胶含水量高(王玲等,2013),导致气溶胶折射指数$m_r$较低,更接近于水的折射指数1.33(Dubovik 等,2002)。复折射指数虚部$m_i$在数值上也呈现出随着灰霾增加而减小的趋势,清洁大气下约为0.04,而整个灰霾过程均值为0.01,并随着污染逐步清除而增大,这说明在灰霾污染中气溶胶吸收作用有所减弱。这与灰霾过程中硫酸盐、硝酸盐等(典型$m_i$值接近于0)散射性二次气溶胶含量的增加有关(魏鹏 等,2013)。

(4)不对称因子

不对称因子$g$主要反映气溶胶前向散射的比例,$g$越接近于1说明前向散射比例越大,$g$越接近于-1说明后向散射比例越大,$g=0$时对应前后向散射均等的情况。本次灰霾过程中$g$值随灰霾的发展逐渐增大,在污染顶峰1月13日出现最大值0.72,之后随污染逐渐清除而减小。清洁天气下不对称因子$g$均值约为0.58(1月9日、17日均值),说明本地区气溶胶前向散射比例大于其他方向散射;而整个灰霾污染过程均值约为0.67,高于清洁天气条件下$g$值约15.5%,说明在灰霾条件下气溶胶粒子前向散射比例更高。这可能与气溶胶粒子发生吸湿增长,体积增大相关(廖国男,2002)。

(5)气溶胶粒子体积谱分布

图4按照第二次灰霾污染过程显示了气溶胶粒子体积谱分布,表2则是在此基础上进一步计算粗细模态气溶胶体积浓度(Volume Concentration)的结果。可以看出,1月9日为清洁大气,气溶胶粒子整体体积浓度较低,440 nm处AOD为0.26±0.08,粒子谱呈现双峰模态分布,细、粗峰值半径分别为0.1 μm和3.9 μm,并且细粗模态气溶胶体积浓度比为0.82,说明北京地区清洁天气下气溶胶粒子体积谱分布中粗模态为主模态(于兴娜 等,2012)。之后两天随着灰霾污染的开始与发展,气溶胶粒子体积浓度增大,440 nm处AOD分别为0.58±0.04与1.47±0.19。这是由于灰霾污染下天气系统稳定,污染物难以扩散而不断累积造成的。粒子谱分布仍然为双峰分布,但细模态增幅更大。到11日时细粗模态气溶胶体积浓度比增加到2.68,同时细粗模态峰值半径分别变为0.3 μm和2.9 μm。1月13日,灰霾污染达到顶峰,440 nm处AOD达2.94,颗粒物总体积浓度约为1月9日的8.7倍,粒子谱呈现为单峰积聚模态,峰值半径为0.43 μm,细模态气溶胶体积浓度约占总体积浓度的90.5%。在污染增多期间细模态气溶胶峰值半径不断增大,这可能是由于灰霾期间较高的相对湿度使水溶性气溶胶粒子发生吸湿增长导致(Eck 等,2005)。之后在1月14日

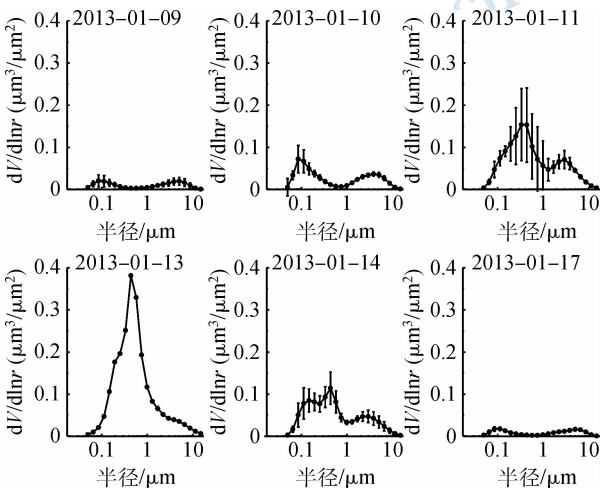


图4 第2次灰霾污染过程气溶胶粒子体积谱分布

**表2 第2次灰霾污染过程中细模态、粗模态气溶胶体积浓度、体积浓度比值(日均值)和AOD(440 nm,日均值)**

| 日期 | 细模态体积浓度/($\mu m^3/\mu m^2$) | 粗模态体积浓度/($\mu m^3/\mu m^2$) | 细/粗模态比值 | AOD(440 nm) |
|---|---|---|---|---|
| 1月9日 | 0.031±0.014 | 0.038±0.015 | 0.82 | 0.26±0.08 |
| 1月10日 | 0.090±0.024 | 0.065±0.009 | 1.38 | 0.58±0.04 |
| 1月11日 | 0.279±0.143 | 0.104±0.009 | 2.68 | 1.47±0.19 |
| 1月13日 | 0.545 | 0.057 | 9.56 | 2.94 |
| 1月14日 | 0.202±0.058 | 0.084±0.024 | 2.39 | 1.10±0.21 |
| 1月17日 | 0.025±0.005 | 0.026±0.005 | 0.95 | 0.21±0.08 |

下午至夜间出现降雪，颗粒物发生沉降，气溶胶粒子整体体积降低，440 nm 处 AOD 降至 1.10±0.21，粒子谱分布恢复为双峰模态，细粗模态峰值半径分别为 0.15 μm 与 2.9 μm，但这一过程中细模态仍然超过粗模态，体积浓度比为 2.39。1 月 17 日灰霾污染基本清除，大气中颗粒物含量较低，达到与 1 月 9 日相当的水平，440 nm 处 AOD 也达到本次过程的最低值 0.21±0.08。气溶胶体积谱分布呈现出细粗模态比例相近的双峰模态，峰值半径分别为 0.1 μm 与 5.0 μm，细粗模态体积浓度比降为 0.95，细模态气溶胶体积浓度略低于粗模态。上述整个污染过程说明本次灰霾主要污染物是细粒子(直径小于 1.0 μm)，粗粒子虽然在灰霾中也有所增长，但增幅较小。另外，这次灰霾过程中细粗模态气溶胶比例与 440 nm 处 AOD 变化趋势一致性较好，进一步说明在该污染过程中总光学厚度中细模态气溶胶有主要贡献。这一点从 Dubovik 等人(2002)得到的城市工业型气溶胶 440 nm 处 AOD 与细模态体积浓度的相关性高于粗模态的结论也可以得到证明。

## 4 结 论

针对北京地区 2013 年 1 月份的严重灰霾污染事件，基于太阳-天空辐射计 CE318 地基遥感观测数据，计算污染期间的气溶胶光学厚度和 Ångström 指数，并且反演了单次散射反照率、复折射指数、粒子谱分布和不对称因子等气溶胶参数，据此详细分析了严重灰霾污染过程中气溶胶的光学和微物理特性，得到以下结论：

(1)2013 年 1 月北京地区灰霾污染期间，气溶胶光学厚度较大，440 nm 处的 AOD 均值达到 0.87，约是同时期清洁天气下的 4 倍(0.87/0.22)，在个别严重污染天气下高达 2.94(1 月 13 日)和 3.29(1 月 27 日)。

(2)气溶胶光学参数与灰霾过程密切相关。灰霾过程中随污染的加剧，$\alpha$ 由于气溶胶粒子吸湿增长从污染前的 1.3 下降到污染时的 0.95；气溶胶吸收作用减弱，$m_i$ 均值由污染前的 0.04 下降为污染过程中的 0.01；气溶胶散射作用增强，清洁和灰霾条件下 SSA 均值分别为 0.73 和 0.92，对应的 g 均值分别为 0.58 与 0.67，说明气溶胶前向散射比例也随污染加剧而有所增强。

(3)灰霾污染过程中细模态气溶胶体积比例较高，最高达 90.5%。该过程中气溶胶模态分布有明显的变化，细粗模态气溶胶比例随污染程度加剧而增大，细模态气溶胶的平均峰值半径随 AOD 增大而增大，清楚表明了灰霾过程中颗粒物的吸湿增长效应。粗模态的平均峰值半径随 AOD 增大表现出减小趋势。灰霾污染最严重时气溶胶粒子体积谱分布呈现出单峰模态，峰值半径约为 0.43 μm。

**志 谢** 感谢中国气象局公共气象服务中心协助提供的气象观测资料。

## 参考文献(References)

Dubovik O, Smirnov A, Holben B N, King M D, Kaufman Y J, Eck T F and Slutsker I. 2000. Accuracy assessments of aerosol optical properties retrieved from Aerosol Robotic Network (AERONET) Sun and sky radiance measurements. Journal of Geophysical Research, 105(D8): 9791-9806 [DOI: 10.1029/2000JD900040]

Dubovik O, Holben B N, Eck T F, Smirnov A, Kaufman Y J, King M D, Tanré D and Slutsker I. 2002. Variability of absorption and optical properties of key aerosol types observed in worldwide locations. Journal of the Atmospheric Sciences, 59(3): 590-608 [DOI: 10.1175/1520-0469(2002)059<0590:VOAAOP>2.0.CO;2]

Dubovik O, Sinyuk A, Lapyonok T, Holben B N, Mishchenko M, Yang P, Eck T F, Volten H, Muñoz O, Veihelmann B, van der Zande W J, Leon J F, Sorokin M and Slutsker I. 2006. Application of spheroid models to account for aerosol particle nonsphericity in remote sensing of desert dust. Journal of Geophysical Research, 111(D11) [DOI: 10.1029/2005JD00661 9]

Eck T F, Holben B N, Reid J S, Dubovik O, Smirnov A, O'Neill N T, Slutsker I and Kinne S S. 1999. Wavelength dependence of the optical depth of biomass burning, urban, and desert dust aerosols. Journal of Geophysical Research, 104(D24): 31333-31349 [DOI: 10.1029/1999JD900923]

Eck T F, Holben B N, Dubovik O, Smirnov A, Goloub P, Chen H B, Chatenet B, Gomes L, Zhang X Y, Tsay S C, Ji Q, Giles D and Slutsker I. 2005. Columnar aerosol optical properties at AERONET sites in central eastern Asia and aerosol transport to the tropical mid-Pacific. Journal of Geophysical Research, 110(D6) [DOI: 10.1029/2004jd005274]

Li Z, Gu X, Wang L, Li D, Li K, Dubovik O, Schuster G, Goloub P, Zhang Y, Li L, Xie Y, Ma Y and Xu H. 2013. Aerosol physical and chemical properties retrieved from ground-based remote sensing measurements during heavy haze days in Beijing Winter. Atmospheric Chemistry and Physics Discussion, 13(2): 5091-5122 [DOI: 10.5194/acpd-13-5091-2013]

李正强, 许华, 张莹, 张玉环, 陈澄, 李东辉, 李莉, 侯伟真, 吕阳, 顾行发. 2013. 北京区域2013 严重灰霾污染的主被动遥感监测. 遥感学报, 17(4): 919-928 [DOI:10.11834/jrs.20133066]

廖国男. 2002. 大气辐射导论 第二版. 北京: 气象出版社: 6-8

闵敏, 王普才, 宗雪梅, 夏俊荣, 孟晓艳. 2009. 灰霾过程中的气溶胶特性观测研究. 气候与环境研究, 14(2): 153-160

Tanré D, Deroo C, Duhaut P, Herman M, Morcrette J J, Perbos J and De-

schamps P Y. 1990. Technical note Description of a computer code to simulate the satellite signal in the solar spectrum: the 5S code. International Journal of Remote Sensing, 11(4): 659-668 [DOI: 10.1080/01431169008955048]

王玲, 李正强, 马roman, 李莉, 魏鹏. 2013. 基于太阳-太空辐射计的遥感观测反演北京冬季灰霾气溶胶化学成分含量. 遥感学报, 17(4): 944-958 [DOI:10.11834/jrs.20133059]

王喜全, 杨婷, 王自发. 2011. 灰霾污染的跨控制区影响一次京津冀与东北地区灰霾污染个案分析. 气候与环境研究, 16(6): 690-696

魏鹏, 王堰, 谢一凇, 李正强, 张莹, 许华. 2013. 灰霾污染状况下气溶胶化学组成及辐射效应的遥感估算. 遥感学报, 17(4): 1021-1031 [DOI:10.11834/jrs.20133080]

徐政, 李卫军, 于阳春, 王新锋, 周声圳, 王文兴. 2011. 济南秋季霾与非霾天气下气溶胶光学性质的观测. 中国环境科学, 31(4): 546-552

Yan P, Tang J, Huang J, Mao J, Zhou X, Liu Q, Wang Z and Zhou H. 2008. The measurement of aerosol optical properties at a rural site in Northern China. Atmospheric Chemistry and Physics, 8(8): 2229-2242

于兴娜, 李新妹, 登增然登, 德庆央宗, 袁帅. 2012. 北京雾霾天气期间气溶胶光学特性. 环境科学, 33(4): 1057-1062

# 遥感学报

启功先生创刊题名

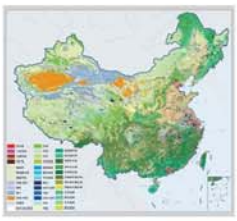

## 封面说明

About the Cover

2010年中国土地覆被遥感监测数据集（ChinaCover2010）

The China National Land Cover Data for 2010 (ChinaCover2010)

2010年中国土地覆被遥感监测数据集（ChinaCover2010）由中国科学院遥感与数字地球研究所联合其他9个单位历时两年完成，应用30 m空间分辨率的环境星（HJ-1A/1B）数据，利用联合国粮农组织（FAO）的LCCS分类工具，构建了适用于中国生态特征的38类土地覆被分类系统，采用基于超算平台的数据预处理、面向对象的自动分类、地面调查获得的10万个野外样本以及雷达数据辅助分类相结合的方法，数据精度达到85%。ChinaCover2010主要基于国产卫星影像，将遥感与生态紧密结合，充足的野外样点以及严格的产品质量控制在最大程度上保证了数据的精度，可为中国生态环境变化评估以及生态系统碳估算提供基础数据支撑。（网址：http://www.chinacover.org.cn）

The China National Land Cover Data for 2010 (ChinaCover2010) has been completed after two years of team effort by the Institute of Remote Sensing and Digital Earth (RADI), Chinese Academy of Sciences (CAS), together with nine other institutions' participation. The HJ-1A/1B satellite at 30 m resolution is main data source. Based on the landscape features in China, 38 land cover classes have been defined using UN FAO Land Cover Classification System (LCCS). Super computers were used in the data preprocessing. An object-oriented method and a thorough field survey (about 100000 field samples) were used in the land cover classification, with radar imagery as auxiliary data. The overall accuracy of ChinaCover2010 is around 85%. Mainly based on domestic imagery, the products take advantage of various in situ data and strict quality control. ChinaCover2010 is a good dataset for ecological environment change assessment and terrestrial carbon budget studies. (Website: http://www.chinacover.org.cn)


# 遥感学报

# JOURNAL OF REMOTE SENSING

YAOGAN XUEBAO（双月刊　1997年创刊）

第17卷　第4期　2013年7月25日

(Bimonthly, Started in 1997)

Vol.17 No.4 July 25, 2013

| | | | |
|---|---|---|---|
| 主　管 | 中国科学院 | Superintended by | Chinese Academy of Sciences |
| 主　办 | 中国科学院遥感与数字地球研究所<br>中国地理学会环境遥感分会 | Sponsored by | Institute of Remote Sensing and Digital Earth,CAS<br>The Associate on Environment Remote Sensing of China |
| 主　编 | 顾行发 | Editor-in-Chief | GU Xing-fa |
| 编　辑 | 《遥感学报》编委会<br>北京市安外大屯路中国科学院遥感与数字地球研究所<br>邮编：100101　电话：86-10-64806643<br>http://www.jors.cn<br>E-mail:jrs@irsa.ac.cn | Edited by | Editorial Board of Journal of Remote Sensing<br>Add: P.O.Box 9718, Beijing 100101, China<br>Tel: 86-10-64806643<br>http://www.jors.cn<br>E-mail: jrs@irsa.ac.cn |
| 出　版 | 科学出版社 | Published by | Science Press |
| 印刷装订 | 北京科信印刷有限公司 | Printed by | Beijing Kexin Printing Co. Ltd. |
| 总 发 行 | 科学出版社<br>北京东黄城根北街16号<br>邮政编码：100717<br>电话：86-10-64017032<br>E-mail:sales_journal@mail.sciencep.com | Distributed by | Science Press<br>Add: 16 Donghuangchenggen North Street, Beijing 100717, China<br>Tel: 86-10-64017032<br>E-mail: sales_journal@mail.sciencep.com |
| 国外发行 | 中国国际图书贸易总公司<br>北京399信箱　邮政编码：100044 | Overseas distributed by | China International Book Trading Corporation<br>Add: P.O.Box 399, Beijing 100044, China |

中国标准连续出版物号：ISSN 1007-4619 / CN 11-3841/TP

CODEN YXAUAB

国内邮发代号：82-324

国外发行代号：BM 1002

定价：70.00元

ISSN 1007-4619

国内外公开发行